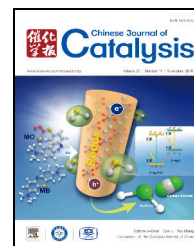


available at www.sciencedirect.comjournal homepage: www.elsevier.com/locate/chnjc

Article

Photocatalytic activity of TiO₂ supported SiO₂-Al₂O₃ aerogels prepared from industrial fly ash

Hui-Long Wang^a, Hui-Ping Qi^a, Xiao-Na Wei^a, Xiao-Yu Liu^b, Wen-Feng Jiang^{a,*}^a Department of Chemistry, Dalian University of Technology, Dalian 116024, China^b Experimental Center of Chemistry, Dalian University of Technology, Dalian 116024, China

ARTICLE INFO

Article history:

Received 12 July 2016

Accepted 3 September 2016

Published 5 November 2016

Keywords:

Titania

SiO₂-Al₂O₃ aerogel

Composite photocatalyst

Industrial fly ash

2-sec-butyl-4,6-dinitrophenol

Wastewater treatment

ABSTRACT

A ternary composite of TiO₂ and a SiO₂-Al₂O₃ aerogel with good photocatalytic activity was prepared by a simple sol-gel method with TiO₂ nanoparticles and SiO₂-Al₂O₃ aerogels derived from industrial fly ash. The structural features of the TiO₂/SiO₂-Al₂O₃ aerogel composite were investigated by X-ray powder diffraction, Fourier transform infrared spectroscopy, transmission electron microscopy, gas adsorption measurements and diffuse reflectance UV-visible spectroscopy. The optimal conditions for photocatalytic degradation of 2-sec-butyl-4,6-dinitrophenol (DNBP), included an initial DNBP concentration of 0.167 mmol/L at pH = 4.86 with a catalyst concentration of 6 g/L, under visible light irradiation for 5 h. A plausible mechanism is proposed for the photocatalytic degradation of DNBP. Our composite showed higher photocatalytic activity for DNBP degradation than that of pure TiO₂. This indicates that this material can serve as an efficient photocatalyst for degradation of hazardous organic pollutants in wastewater.

© 2016, Dalian Institute of Chemical Physics, Chinese Academy of Sciences.
Published by Elsevier B.V. All rights reserved.

1. Introduction

2-sec-Butyl-4,6-dinitrophenol (DNBP), one of the most important alkyl dinitrophenols, is widely used in the petrochemical industry as a polymerization inhibitor for vinyl aromatics and in agriculture as a herbicide [1,2]. Owing to its high use in industry and agriculture, it is regularly detected in aquatic environments. Although there are benefits to using DNBP, it is now considered to exert negative influences on the environment owing to its toxicity, carcinogenicity and mutagenicity. DNBP is on a US Environmental Protection Agency blacklist for priority pollutants in water [3]. Although there has been much research on the removal of nitrophenol contaminants from the environment, there are only a few reports on DNBP degradation. DNBP is highly chemically stable, toxic and persistent in

ecosystems [4–6]. Thus, removal of DNBP from aqueous solution has attracted considerable research interest.

Research on semiconducting materials that mediate photocatalytic degradation of organic pollutants for environmental remediation is an area of growing interest [7,8]. Among semiconductor photocatalysts, TiO₂ is widely used for the destruction of organic pollutants because of its relatively high catalytic reactivity, good physical and chemical stability, low-toxicity and cost-effectiveness. TiO₂ generates electron and hole pairs (e⁻/h⁺) upon irradiation of light energy equal to or greater than its band gap energy. If charge separation occurs, the photo-generated electrons and holes may migrate to the catalyst surface and participate in redox reactions with adsorbed species [9,10]. However, TiO₂ suffers from a low adsorption capacity, rapid recombination of electron-hole pairs, and the difficul-

* Corresponding author. Tel: +86-411-84708941; Fax: +86-411-84708590; E-mail: dlutjiangwf@163.com

This work was supported by the National Natural Science Foundation of China (21377018), the Natural Science Foundation of Liaoning Province of China (2013020116) and the Fundamental Research Funds for the Central Universities (DUT15ZD240).

DOI: 10.1016/S1872-2067(16)62546-9 | <http://www.sciencedirect.com/science/journal/18722067> | Chin. J. Catal., Vol. 37, No. 11, November 2016

ty of recycling the catalyst. These issues have limited the use of TiO_2 nanoparticles in practical applications such as wastewater treatment. Various attempts have been made to enhance the absorption capacity and photocatalytic activity of TiO_2 nanoparticles. TiO_2 supported on porous adsorbent materials is one approach that has drawn much attention. Supported TiO_2 catalysts may allow the pollutant to be concentrated near the TiO_2 particles, mediate adsorption of intermediates formed during degradation, and allow the catalyst to be recovered and reused [11–14]. Among support materials for TiO_2 , aerogels based on silica and other metal oxides (alumina, zirconia, tungsten oxide, or a mixtures of these oxides) are considered attractive candidates owing to their special physicochemical features, including high specific surface area, porous structure, high thermal stability, easily tunable chemical properties, environmentally-friendly nature and photo-stable inorganic frameworks [15]. Recently, a silica aerogel-supported TiO_2 has been used as a catalyst in photocatalytic processes [16]. The physicochemical properties of silica aerogel-supported TiO_2 catalysts depended on their synthesis conditions and the degree of interaction between the TiO_2 and silica aerogel support. The strong electric field present in the framework of these supports can minimize electron-hole recombination and also allows pollutants to be concentrated near the TiO_2 particles [17,18].

Aerogels based on silica and other metal oxides are traditionally prepared via supercritical drying processes using silicate ester, aluminosilica gel and other organometallic compounds as raw materials [19–21]. However, the precursors and supercritical drying techniques used for preparing the aerogels are costly and dangerous, which limits the practical and commercial viability of such supports. Fly ash is a coal combustion by-product consisting of an alumina-silica mixture with smaller amounts of iron, calcium, sodium and potassium [22].

The objective of our work was to investigate a $\text{TiO}_2/\text{SiO}_2\text{-Al}_2\text{O}_3$ aerogel composite catalyst for degradation of persistent organic contaminants in wastewater. Here, we report the synthesis of $\text{SiO}_2\text{-Al}_2\text{O}_3$ binary aerogels derived from industrial fly ash, synthesized by an ambient pressure drying method. The prepared $\text{SiO}_2\text{-Al}_2\text{O}_3$ binary aerogels were used as a support matrix for TiO_2 nanoparticles, to create a composite material with a high adsorption capacity and enhanced photocatalytic activity. The photocatalytic degradation of DNBP over our $\text{TiO}_2/\text{SiO}_2\text{-Al}_2\text{O}_3$ aerogel composite was tested under visible light irradiation.

2. Experimental

2.1. Materials and reagents

A representative sample of the fly ash was collected from the Zhungeer coal mine (Inner Mongolia, China). The constituents of the fly ash used in the experiments were as follows: SiO_2 48.16%, Al_2O_3 21.68%, Fe_2O_3 5.64%, TiO_2 1.12%, CaO 2.04%, MgO 1.08%, K_2O 0.50%, Na_2O 0.12%, MnO_2 0.02%, SO_3 0.82%, and P_2O_5 0.54%. The loss on ignition (LOI) was determined to be 18.22%. DNBP was used as a model alkyl dinitrophenol pollutant and obtained from Retell Fine Chemical Co. Ltd. (Tianjin,

China). Tetrabutyl titanate (TBOT, $\geq 98.0\%$), polyethylene glycol 400 (PEG-400) and trimethylchlorosilane (TMCS, $\geq 98.0\%$) were obtained from Sinopharm Chemical Reagent Co. Ltd., China. All other reagents used in this study, were AR grade obtained from Tianjin Kermel Chemical Reagents Co. Ltd., China. All reagents were used as received without further purification. Double distilled water was used to prepare solutions in the experiments.

2.2. Preparation of materials

2.2.1. Preparation of $\text{SiO}_2\text{-Al}_2\text{O}_3$ aerogel samples from fly ash

Fly ash sample and sodium carbonate were well mixed at a mass ratio of 1:1 and calcined at 900 °C for 3 h in a muffle furnace. After cooling to room temperature, a HCl solution (5.0 mol/L) was added to the calcined product and stirred for 3 h at room temperature to produce an aluminosilica-sol. The mixture was then filtered and the homogeneous aluminosilica-sol was collected. The pH of the obtained aluminosilica-sol was adjusted to 10.0–11.0 using a NaOH solution (5.0 mol/L) for gelation. After 30 min the aluminosilica wet gels produced were aged for 6 h at 50 °C to strengthen the gel network structure, and then solvent exchanged with absolute ethanol at 50 °C for 24 h. Surface modification was performed by immersing the aluminosilica gels in TMCS/ethanol/cyclohexane solutions for 48 h. Surface modification and solvent exchange of the aluminosilica gels were performed simultaneously and the molar ratio of TMCS:ethanol:cyclohexane was 2:5:9. The aluminosilica gels were thoroughly washed with cyclohexane to remove unreacted agents and reaction products and the surface-modified gel samples were left to dry for 24 h. The gels were dried at 80 °C in an oven at atmospheric pressure. The resultant aluminosilica gels were stored in a vacuum desiccator prior to further use.

2.2.2. Preparation of $\text{TiO}_2/\text{SiO}_2\text{-Al}_2\text{O}_3$ aerogel composite

The $\text{TiO}_2/\text{SiO}_2\text{-Al}_2\text{O}_3$ aerogel composite was prepared through an acid-catalyzed sol-gel method. A typical procedure was as follows: 0.093 g of the as-obtained $\text{SiO}_2\text{-Al}_2\text{O}_3$ aerogel was added to a mixture of 5 mL absolute ethanol, 2 mL acetic acid and 2.5 mL water. The mixture was sonicated for 30 min at room temperature to obtain a suspension. A 5-mL portion of TBOT was added gradually to a mixture of 10 mL anhydrous ethanol and 3 mL acetic acid under continuous stirring to prepare the titanium precursor. The titania-sol was slowly added to the suspension of $\text{SiO}_2\text{-Al}_2\text{O}_3$ aerogel to initiate the hydrolysis reaction. After complete hydrolysis of the titanium precursor, the colloidal solution was continuously stirred for 2 h until the formation of a TiO_2 gel. After aging for at least 12 h at room temperature, the resulting sample was then dried at 110 °C for 12 h, and calcined at 300 °C for 1 h and 450 °C for 2 h in a muffle furnace under ambient atmosphere. The resultant $\text{TiO}_2/\text{SiO}_2\text{-Al}_2\text{O}_3$ aerogel composite materials were stored in a vacuum desiccator prior to further use.

2.3. Characterization

The X-ray powder diffraction (XRD) patterns of the materials were measured by a Rigaku D/MAX-2000 diffractometer using Cu K_{α} radiation operating at 30 mA and 40 kV with a scan rate of $2\theta = 4.8^{\circ}/\text{min}$. Fourier transform infrared spectra (FT-IR) of the samples within the 400–4000 cm^{-1} frequency range were measured on a Nicolet Avatar 360 FT-IR infrared spectrometer using conventional KBr pellets. The particle size and morphologies of the samples were also determined with a transmission electron microscope (TEM, FEI Tecnai G220S-TWIN, America). The UV-vis diffuse reflectance spectra (UV-vis/DRS) of the catalysts in the range 200–800 nm were measured on a JASCO UV-550 ultraviolet spectrometer equipped with an integrating sphere with BaSO_4 as a reference. The specific surface areas of the catalysts were determined by the BET method with a Micromeritics ASAP 2010 apparatus. All the samples were previously degassed at 350 $^{\circ}\text{C}$ for 12 h.

2.4. Zero point charge (pH_{zpc}) measurement

The zero point charge (pH_{zpc}) of the $\text{TiO}_2/\text{SiO}_2\text{-Al}_2\text{O}_3$ aerogel catalyst was measured with 10-mL portions of NaCl aqueous solution (0.05 mol/L) that were adjusted to pH values in the range 2–11 by either HCl or NaOH solutions (0.1 mol/L) [23]. N_2 gas was bubbled through the NaCl solutions to remove dissolved CO_2 until the initial pH stabilized. After determination of the initial pH value, the solutions were mixed with 0.03 g of the catalyst sample for 24 h and the final pH of the solutions was then measured. The pH_{zpc} value was defined as the pH at which the initial and final pH values were equal. The pH of the solution was measured by using a Mettler-Toledo (model Delta 320-S) digital pH meter.

2.5. Photocatalytic degradation of DNBP

Photocatalytic degradation of DNBP was performed in a XPA-7 photochemical reactor (Xujiang Electromechanical Plant, Nanjing, China). Cylindrical quartz photochemical reactors of 22 cm \times 2 cm (height \times diameter) were vertically placed at a fixed distance (3.5 cm) from a 500 W Xenon lamp (Institute of Electric Light Source, Beijing) as light source to mimic solar irradiation. For the irradiation experiments, an aqueous solution of DNBP (40 mL) and the photocatalyst were added to the photoreactor. The resultant mixture was stirred continuously in the dark for at least 2 h to ensure the adsorption/desorption equilibrium of DNBP was established. The suspensions were then irradiated by the xenon lamp with the transmission of wavelengths below 380 nm limited using glass filters, while continuous purging the reactor with air. Aliquots were withdrawn at specific time intervals during the degradation experiments and analyzed after centrifugation for 5 min at 3000 r/min to completely remove any solid particles. The filtrates were subjected to UV-visible spectrophotometric analysis to monitor the concentration of DNBP at various time intervals at a wavelength of 271 nm [24]. The mineralization of DNBP was monitored by measuring the total organic carbon (TOC) with an Elementary Analyzer (Multi N/C 2100S, Analytikjena) by direct injection of the aqueous solution after the photocatalysis

reaction. The GC/MS system (Agilent 6890 GC and 5793 MS) was used to identify the intermediate products formed during the photooxidative process. The carrier gas flow rate was 0.5 mL/min and the oven temperature was programmed as follows: isothermal at 40 $^{\circ}\text{C}$ for 5 min, from 40 to 280 $^{\circ}\text{C}$ at 5 $^{\circ}\text{C}/\text{min}$, and isothermal at 280 $^{\circ}\text{C}$ for 1 min.

3. Results and discussion

3.1. Characterization results

Fig. 1 illustrates the XRD patterns of pure TiO_2 , $\text{SiO}_2\text{-Al}_2\text{O}_3$ aerogel, and $\text{TiO}_2/\text{SiO}_2\text{-Al}_2\text{O}_3$ aerogel composite. A series of intensified anatase diffraction peaks were observed in Fig. 1(1). The XRD pattern of the $\text{SiO}_2\text{-Al}_2\text{O}_3$ aerogel (Fig. 1(2)) showed a broad, weak peak in the range 15–30 $^{\circ}$, attributable to amorphous SiO_2 . The non-crystalline diffraction peaks of SiO_2 were so broad that peaks from Al_2O_3 were not visible in the pattern. According to Fig. 1(3), the XRD pattern of the $\text{TiO}_2/\text{SiO}_2\text{-Al}_2\text{O}_3$ aerogel composite contained the same characteristic peaks as anatase-type TiO_2 , which indicated that the introducing the $\text{SiO}_2\text{-Al}_2\text{O}_3$ aerogel only slightly weakened the diffraction patterns of pure TiO_2 .

Fig. 2 shows FT-IR spectra of the $\text{SiO}_2\text{-Al}_2\text{O}_3$ aerogel, pure TiO_2 and $\text{TiO}_2/\text{SiO}_2\text{-Al}_2\text{O}_3$ aerogel composite. In these spectra, the broad absorption peaks at 3440 and 1630 cm^{-1} were attributed to stretching and bending vibrations of surface absorbed water and hydroxyl groups. The $\text{SiO}_2\text{-Al}_2\text{O}_3$ aerogel samples (Fig. 2(1)) showed characteristic peaks of Si–O–Si asymmetric and symmetric vibrations at 1080 and 762 cm^{-1} [25]. The peak at 847 cm^{-1} was attributed to a stretching vibration of Al–O–Al. The absorption peaks centered around 2960 and 1258 cm^{-1} corresponded to stretching and deformation modes of C–H and Si–C bonds, respectively [26]. The absorption bands of the Si–C bond and C–H bonds confirmed the modification of the $\text{SiO}_2\text{-Al}_2\text{O}_3$ aerogel samples. As shown in Fig. 2(2), the low frequency absorption in the region 500–700 cm^{-1} can be assigned to a stretching vibration of Ti–O–Ti. FT-IR spectra of pure TiO_2 and $\text{TiO}_2/\text{SiO}_2\text{-Al}_2\text{O}_3$ aerogel composites showed a similar shape. In Fig. 2(3), the characteristic absorp-

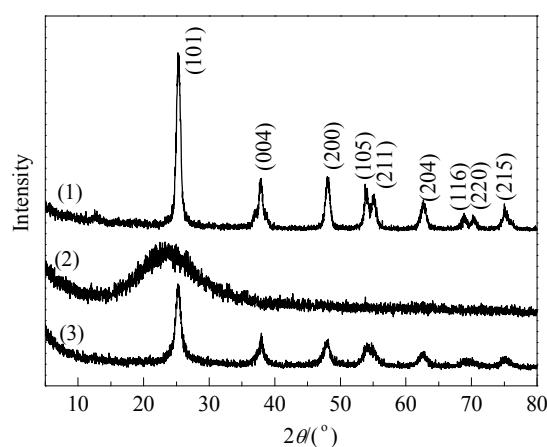


Fig. 1. XRD patterns of (1) TiO_2 , (2) $\text{SiO}_2\text{-Al}_2\text{O}_3$ aerogel, and (3) $\text{TiO}_2/\text{SiO}_2\text{-Al}_2\text{O}_3$ aerogel composite.

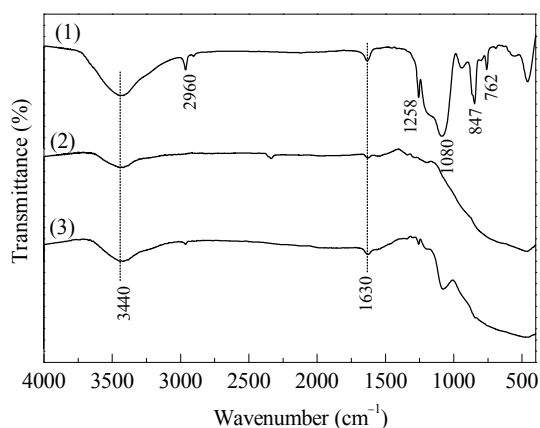


Fig. 2. FT-IR spectra of (1) $\text{SiO}_2\text{-Al}_2\text{O}_3$ aerogel, (2) TiO_2 , and (3) $\text{TiO}_2/\text{SiO}_2\text{-Al}_2\text{O}_3$ aerogel composite.

tion peaks of the stretching vibrations of Si–O–Si and Ti–O–Ti are visible, demonstrating the successful synthesis of $\text{TiO}_2/\text{SiO}_2\text{-Al}_2\text{O}_3$ aerogel composite samples.

Fig. 3 shows TEM images of the as-prepared $\text{SiO}_2\text{-Al}_2\text{O}_3$ aerogel and $\text{TiO}_2/\text{SiO}_2\text{-Al}_2\text{O}_3$ aerogel composite. Fig. 3(a) shows that the $\text{SiO}_2\text{-Al}_2\text{O}_3$ aerogel was porous with a regular network structure. The $\text{TiO}_2/\text{SiO}_2\text{-Al}_2\text{O}_3$ aerogel composite (Fig. 3(b)) featured TiO_2 particles ranging in size from 10 to 30 nm dispersed evenly on the $\text{SiO}_2\text{-Al}_2\text{O}_3$ aerogel. The $\text{SiO}_2\text{-Al}_2\text{O}_3$ aerogels improved the dispersion and reduced the average size of the TiO_2 particle agglomerates. In addition, the structural characteristics of the $\text{SiO}_2\text{-Al}_2\text{O}_3$ aerogel indicate its potential for enhancing adsorption of organic pollutants.

Fig. 4 shows a nitrogen adsorption-desorption isotherm of an as-synthesized $\text{TiO}_2/\text{SiO}_2\text{-Al}_2\text{O}_3$ aerogel composite sample, which showed a type IV-like isotherm with a type H1 hysteresis loop. This finding suggests the presence of mesoporosity in the $\text{TiO}_2/\text{SiO}_2\text{-Al}_2\text{O}_3$ aerogel composite matrix. According to the results calculated by BET, the surface areas of the TiO_2 , $\text{SiO}_2\text{-Al}_2\text{O}_3$ aerogel and $\text{TiO}_2/\text{SiO}_2\text{-Al}_2\text{O}_3$ aerogel composite samples were 87, 401.4 and 107.8 m^2/g , respectively. The lower surface area of the composite than that of the $\text{SiO}_2\text{-Al}_2\text{O}_3$ aerogel may be explained by TiO_2 particles in the composite shrinking the overall surface area through particle agglomeration and/or blocking pores. However, the $\text{SiO}_2\text{-Al}_2\text{O}_3$ aerogel in the composite gave a higher surface area than that of TiO_2 alone, confirming the supporting role of the $\text{SiO}_2\text{-Al}_2\text{O}_3$ binary aerogels. The high specific surface area of $\text{TiO}_2/\text{SiO}_2\text{-Al}_2\text{O}_3$ aer-

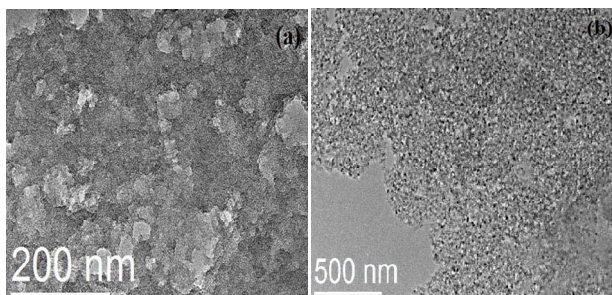


Fig. 3. TEM images of (a) $\text{SiO}_2\text{-Al}_2\text{O}_3$ aerogel and (b) $\text{TiO}_2/\text{SiO}_2\text{-Al}_2\text{O}_3$ aerogel composite.

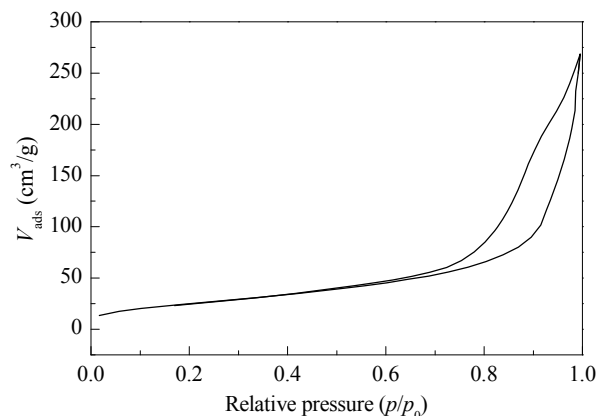


Fig. 4. N_2 adsorption-desorption isotherm of $\text{TiO}_2/\text{SiO}_2\text{-Al}_2\text{O}_3$ aerogel composite.

ogel improved photocatalytic degradation of organic contaminants by allowing better adsorption of reactant molecules. Enhancing the concentration of reactant molecules around the TiO_2 photoactive layer will benefit photocatalytic decomposition of organic pollutants. Reactant molecules are more likely to interact quickly with short-lived hydroxyl radicals that are localized on the $\text{SiO}_2\text{-Al}_2\text{O}_3$ aerogel surface.

Fig. 5 shows UV-vis diffuse reflectance spectra of TiO_2 and the $\text{TiO}_2/\text{SiO}_2\text{-Al}_2\text{O}_3$ aerogel composite in the range of 200–800 nm. There were no major differences in the absorption of the $\text{TiO}_2/\text{SiO}_2\text{-Al}_2\text{O}_3$ aerogel composite compared with that of pure TiO_2 . This indicates that the $\text{SiO}_2\text{-Al}_2\text{O}_3$ aerogels only slightly affected the absorption profile of the TiO_2 . The $\text{TiO}_2/\text{SiO}_2\text{-Al}_2\text{O}_3$ aerogel composite exhibited slight stronger absorption in the visible region than that of the pure TiO_2 samples. This is because the $\text{SiO}_2\text{-Al}_2\text{O}_3$ aerogel ensured a better distribution of the TiO_2 nanoparticles to maximize their photoconversion efficiency. According to the method reported in the literature [27], the band gap energies (E_g) of the $\text{TiO}_2/\text{SiO}_2\text{-Al}_2\text{O}_3$ aerogel composite and pure TiO_2 were calculated to be 3.02 and 3.08 eV, respectively.

3.2. Photocatalytic degradation of DNBP

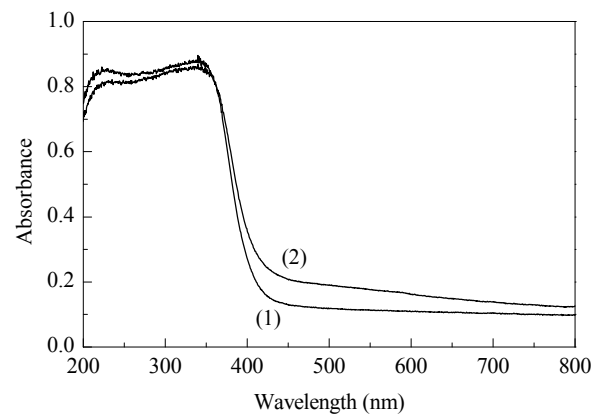


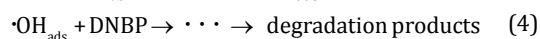
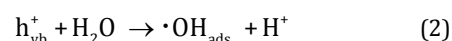
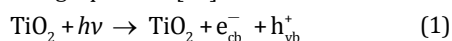
Fig. 5. UV-vis absorption spectra of (1) pure TiO_2 and (2) $\text{TiO}_2/\text{SiO}_2\text{-Al}_2\text{O}_3$ aerogel composite.

The effects of reaction variables such as pH, catalyst concentration, initial concentration of DNBP, irradiation time on the degradation efficiency were investigated.

3.2.1. Effect of pH

Solution pH influences adsorption and dissociation of the substrate, catalyst surface charge, oxidation potential of the valence band and other physicochemical properties of the system. The effect of pH on the photocatalytic degradation efficiency of DNBP was investigated at different pH values in the range 1.86–12.89 and the results are presented in Fig. 6. During these experiments, the pH of the solution was adjusted before light irradiation, but was not controlled during the course of the reaction. The figure shows that the degradation efficiency of DNBP increased as the pH was increased from 1.86 to 4.86. For further increases in pH the degradation efficiency started to decrease. Maximum degradation was obtained at pH = 4.86 (natural pH of DNBP solution) under visible light irradiation.

The solution pH affected the formation of $\cdot\text{OH}$ radicals as illustrated in the following equations [28]:



very low and high pH values disfavor production of $\cdot\text{OH}$ radical because of the high redox potentials of Eqs. (2) and (3). The change in solution pH also affected the TiO_2 surface. The pH-dependence of the surface charge was consistent with the pH_{zpc} of the photocatalyst. The pH_{zpc} value was determined to be approximately 4.76 for the prepared $\text{TiO}_2/\text{SiO}_2\text{-Al}_2\text{O}_3$ aerogel composite (Fig. 6 inset). DNBP exists mainly in its molecular forms in acidic medium, and is more likely to dissociate into anions at higher pH values because the pK_a value of DNBP is 4.62. Consequently, DNBP was more favorably adsorbed to the surface of the $\text{TiO}_2/\text{SiO}_2\text{-Al}_2\text{O}_3$ aerogel composite under weak acidic conditions, resulting in a higher DNBP degradation effi-

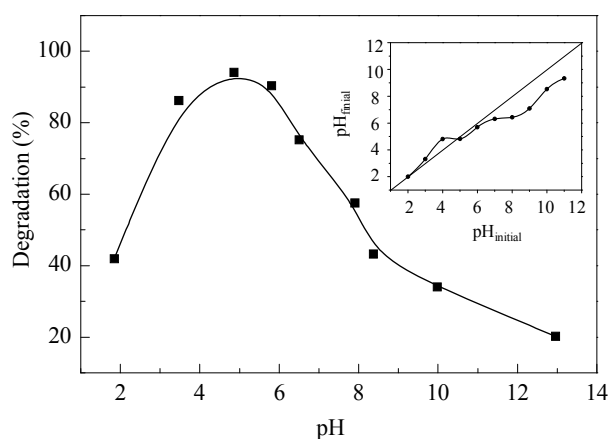


Fig. 6. Effect of pH on photocatalytic degradation of DNBP. Conditions: $C_0(\text{DNBP}) = 0.167 \text{ mmol/L}$, $C(\text{catalyst}) = 6 \text{ g/L}$, irradiation time = 5 h. Inset shows a plot for determination of pH_{zpc} of the as-prepared $\text{TiO}_2/\text{SiO}_2\text{-Al}_2\text{O}_3$ aerogel composite.

ciency.

3.2.2. Effect of catalyst concentration

The effect of catalyst concentration on the photocatalytic degradation efficiency of DNBP was investigated in the concentration range 2–10 g/L. Fig. 7 shows a steady decrease in the DNBP absorption peak for up to 6 g/L of the catalyst. At higher catalyst concentrations the peak absorbance was higher than that at lower concentrations, which indicates the optimal degradation efficiency was achieved at 6 g/L. The enhanced degradation efficiency from 2 to 6 g/L may be attributed to an increased number of available adsorption and catalytic sites on the catalyst surface. However, at high catalyst concentrations, agglomeration of catalyst particles may have increased light scattering and decreased the number of surface active sites, which in turn reduced the production of $\cdot\text{OH}$ radicals and lowered the specific activity of the catalyst. Therefore, an optimized catalyst concentration of 6 g/L was used for further experiments.

3.2.3. Effect of irradiation time

Fig. 8 presents the effect of irradiation time on the photocatalytic degradation of DNBP under the optimized experimental conditions. In a control experiment in which DNBP was illuminated with visible light in the absence of photocatalyst no degradation was observed in solution. This confirmed that the degradation of DNBP occurred predominately via photocatalysis rather than photolysis. The photoactivity of the $\text{TiO}_2/\text{SiO}_2\text{-Al}_2\text{O}_3$ aerogel composite was superior to that of pure TiO_2 . The DNBP photocatalytic degradation efficiencies of pure TiO_2 and $\text{TiO}_2/\text{SiO}_2\text{-Al}_2\text{O}_3$ aerogel composites after irradiation for 5 h were 68.2% and 99.1%, respectively. The enhanced photocatalytic activity of the $\text{TiO}_2/\text{SiO}_2\text{-Al}_2\text{O}_3$ aerogel composite may be attributed to its high capacity for adsorbing organic pollutants. The presence of a mixed TiOSi phase at the $\text{TiO}_2/\text{SiO}_2\text{-Al}_2\text{O}_3$ aerogel interface may also contribute to the high photocatalytic activity of the $\text{TiO}_2/\text{SiO}_2\text{-Al}_2\text{O}_3$ aerogel

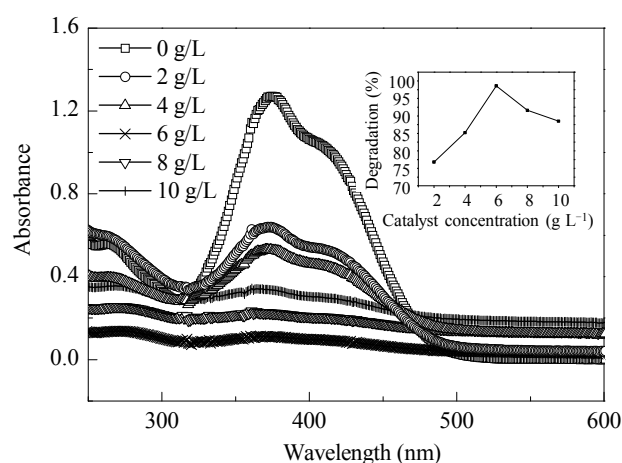


Fig. 7. Time dependent UV-vis absorbance spectra of DNBP degradation in solutions containing different concentrations of $\text{TiO}_2/\text{SiO}_2\text{-Al}_2\text{O}_3$ aerogel composite. Inset shows the effect of $\text{TiO}_2/\text{SiO}_2\text{-Al}_2\text{O}_3$ aerogel concentration on the photocatalytic degradation efficiency of DNBP. Conditions: $C_0(\text{DNBP}) = 0.167 \text{ mmol/L}$, $\text{pH} = 4.86$, irradiation time = 5 h.

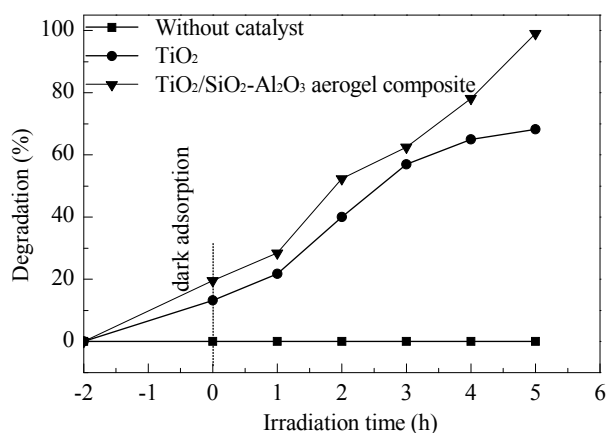


Fig. 8. Effect of irradiation time on the photocatalytic degradation efficiency of DNBP. Conditions: $C_0(\text{DNBP}) = 0.167 \text{ mmol/L}$, pH 4.86, $C(\text{catalyst}) = 6 \text{ g/L}$.

composite [29]. Interfaces of this type have been shown to possess sites with high Brönsted acidity. The strong Brönsted acid sites in the TiOSi region may activate the pollutants towards oxidation.

3.2.4. Effect of initial DNBP concentration and kinetics of photocatalytic degradation

The effect of the DNBP concentration on the photocatalytic degradation efficiency in the presence of the $\text{TiO}_2/\text{SiO}_2\text{-Al}_2\text{O}_3$ aerogel composite catalyst was studied by varying the initial concentration from 0.0629 to 0.2087 mmol/L. The percentage degradation decreased as the initial DNBP concentration was increased. This may be due to blocking of photocatalytic active sites on the catalyst and reduced interaction of light with these sites. At higher DNBP concentrations a larger portion of light was absorbed by the DNBP rather than the catalyst particles, which also reduced the efficiency of the photocatalytic reaction. The photocatalytic reaction on the surface of $\text{TiO}_2/\text{SiO}_2\text{-Al}_2\text{O}_3$ aerogel composite catalyst was a pseudo-first-order reaction and its kinetic equation can be expressed by Langmuir-Hinshelwood model:

$$r = -\frac{dC}{dt} = \frac{k_r KC}{1 + KC} \quad (5)$$

The integrated form of Eq. (6) is:

$$t = \left(\frac{1}{k_r K} \right) \ln \left(\frac{C_0}{C} \right) + \frac{C_0 - C}{k_r} \quad (6)$$

where t refers to the irradiation time, C_0 is initial concentration of DNBP and C is the concentration of DNBP at time t , r represents the rate of degradation, K is the equilibrium constant for the adsorption of DNBP onto the catalyst and k_r reflects the limiting rate of the reaction at the maximum coverage in these experimental conditions.

At low initial DNBP concentrations, the second term in the Eq.(6) becomes insignificant and can be neglected, such that:

$$\ln \left(\frac{C_0}{C} \right) = k_r K t = k_{app} t \quad (7)$$

where k_{app} is the apparent rate constant for the photocatalytic degradation.

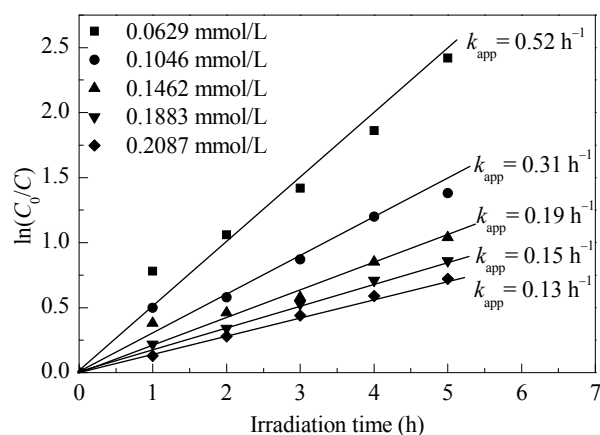


Fig. 9. Degradation kinetic plots for different initial concentrations of DNBP in the presence of $\text{TiO}_2/\text{SiO}_2\text{-Al}_2\text{O}_3$ aerogel composite.

A plot of $\ln(C_0/C)$ vs t gives a straight line, as can be seen in Fig. 9, confirming the applicability of Langmuir-Hinshelwood equation with $k_{app} = 0.52\text{--}0.13 \text{ h}^{-1}$, in the DNBP concentration range 0.0629–0.2087 mmol/L. The apparent rate constant decreased as the initial DNBP concentration was increased in the solution.

3.2.5. Recycling of the catalyst

Recycling and reuse of a photocatalyst is an important factor for its practical application. Thus, we investigated reuse of our $\text{TiO}_2/\text{SiO}_2\text{-Al}_2\text{O}_3$ aerogel composite photocatalyst. After one cycle of DNBP photodegradation, the photocatalyst was filtrated, washed, dried at $80 \text{ }^\circ\text{C}$ for 4 h and then reused for further cycles, while maintaining other reaction conditions. The photocatalytic efficiency of the composite remained above 90% even after 5 cycles (Fig. 10). This indicates that the $\text{TiO}_2/\text{SiO}_2\text{-Al}_2\text{O}_3$ aerogel composite catalyst has good reusability. The reduction in the photocatalytic degradation efficiency over the 5 cycles was likely caused by fouling of the catalyst by organic intermediates generated during the photocatalytic

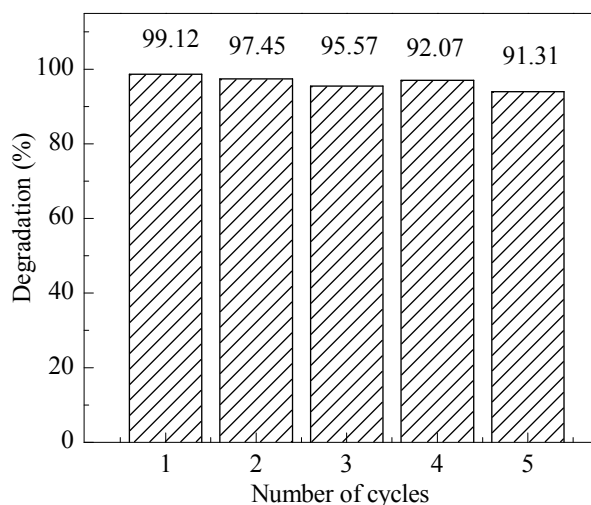


Fig. 10. Results of recycling studies.

reaction, which lowered the $\cdot\text{OH}$ radical production rate.

3.3. Intermediate products

We attempted to identify intermediate products generated during photocatalytic degradation of DNBP, in an aqueous suspension of the $\text{TiO}_2/\text{SiO}_2\text{-Al}_2\text{O}_3$ aerogel composite by GC-MS analysis. Samples were taken at different irradiation time, then filtered and concentrated to 5 mL by rotatory evaporation at 40 °C. The anhydrous residue was dissolved in 25 mL of diethyl ether and sonicated for 10 min. Diethyl ether was removed under reduced pressure, and the residual mass was mixed with 2 mL of methanol and 1 mL of trimethylsulfonium hydroxide. The mixture was then agitated for 10 min at 50 °C and the resulting samples were injected into the GC/MS system (Agilent 6890 GC and 5793 MS) for analysis. From the GC/MS analyses, the main identified intermediates resulting from photocatalytic degradation of DNBP were 3,5-dinitro-salicylaldehyde, 3,5-dinitrocatechol, 4-nitrocatechol. These intermediates may undergo further degradation, eventually leading to aromatic ring opening and formation of aliphatic mono- and dicarboxylic acids, which could eventually be mineralized to CO_2 , H_2O and NO_3^- .

Mineralization of refractory organic pollutants with fast kinetics is highly desirable for pollution control. We measured the TOC content of the DNBP wastewater to evaluate mineralization of the compound before and after the photochemical treatment in the presence of $\text{TiO}_2/\text{SiO}_2\text{-Al}_2\text{O}_3$ aerogel composite photocatalyst. The reduction of TOC in the aqueous DNBP solution after 5 h of visible light irradiation was 70.15% for the

$\text{TiO}_2/\text{SiO}_2\text{-Al}_2\text{O}_3$ aerogel composite photocatalyst. This result confirmed destruction of DNBP and demonstrates the excellent photocatalytic performance of the prepared $\text{TiO}_2/\text{SiO}_2\text{-Al}_2\text{O}_3$ aerogel composite photocatalyst.

4. Conclusions

In summary, TiO_2 nanoparticles loaded on $\text{SiO}_2\text{-Al}_2\text{O}_3$ aerogels from industrial fly ash as raw materials were successfully prepared by a simple sol-gel method. Taking advantages of TiO_2 and $\text{SiO}_2\text{-Al}_2\text{O}_3$ aerogel, the as-obtained $\text{TiO}_2/\text{SiO}_2\text{-Al}_2\text{O}_3$ aerogel composite featured a high adsorption capacity and enhanced photocatalytic activity for degradation of DNBP under visible light irradiation. Satisfactory photocatalytic degradation efficiency could be achieved using optimized operation parameters. The photocatalytic reactions appeared to follow pseudo-first-order kinetics with the reaction rate constant from 0.52 to 0.13 h^{-1} in the DNBP concentration range of 0.0629 to 0.2087 mmol/L. The $\text{TiO}_2/\text{SiO}_2\text{-Al}_2\text{O}_3$ aerogel composite catalyst could be reused with no obvious decline in photocatalytic efficiency observed after five cycles of catalytic degradation. The results of this study show that a $\text{TiO}_2/\text{SiO}_2\text{-Al}_2\text{O}_3$ aerogel composite material can be used as an efficient photocatalyst for removal of organic pollutants from water.

Acknowledgments

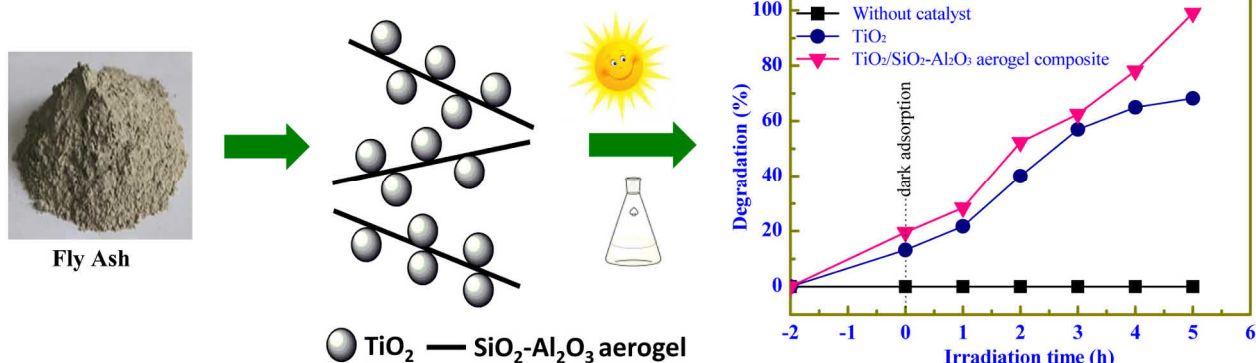
We gratefully acknowledge the financial support provided by the National Natural Science Foundation of China (21377018), the Natural Science Foundation of Liaoning Prov-

Graphical Abstract

Chin. J. Catal., 2016, 37: 2025–2033 doi: 10.1016/S1872-2067(16)62546-9

Photocatalytic activity of TiO_2 supported $\text{SiO}_2\text{-Al}_2\text{O}_3$ aerogels prepared from industrial fly ash

Hui-Long Wang, Hui-Ping Qi, Xiao-Na Wei, Xiao-Yu Liu, Wen-Feng Jiang*
Dalian University of Technology



A ternary composite of $\text{TiO}_2/\text{SiO}_2\text{-Al}_2\text{O}_3$ aerogel with good photocatalytic activity was prepared by a simple sol-gel method with TiO_2 nanoparticles and $\text{SiO}_2\text{-Al}_2\text{O}_3$ aerogels derived from industrial fly ash. The as-prepared composite showed higher photocatalytic activity for 2-sec-butyl-4,6-dinitrophenol (DNBP) degradation than that of pure TiO_2 under visible light irradiation.

ince of China (2013020116) and the Fundamental Research Funds for the Central Universities (DUT15ZD240).

References

- [1] P. Millburn, D. A. Leger, H. O'Neill, J. E. Rishards, J. A. MacLeod, K. MacQuarrie, *Water Qual. Res. J. Can.*, **1995**, 30, 383–397.
- [2] J. I. Nakajima, S. Tanizaki, H. Tomioka, *J. Jpn. Pet. Inst.*, **2003**, 46, 359–367.
- [3] M. Crawford, *Science*, **1986**, 234, 422.
- [4] C. M. Palmeria, *Toxic. Subst. Mech.*, **1999**, 18, 187–204.
- [5] K. L. Takahashi, H. Hojo, H. Aoyama, S. Teramoto, *Reprod. Toxicol.*, **2004**, 18, 581–588.
- [6] H. L. Wang, W. F. Jiang, *Ind. Eng. Chem. Res.*, **2007**, 46, 5405–5411.
- [7] M. A. Fox, M. T. Dulay, *Chem. Rev.*, **1993**, 93, 341–357.
- [8] H. R. Hoffmann, S. T. Martin, W. Choi, D. W. Bahnemann, *Chem. Rev.*, **1995**, 95, 69–96.
- [9] A. Fujishima, X. T. Zhang, D. A. Tryk, *Surf. Sci. Rep.*, **2008**, 63, 515–582.
- [10] A. Di Paola, E. García-López, G. Marci, L. Palmisano, *J. Hazard. Mater.*, **2012**, 211–212, 3–29.
- [11] T. Torimoto, S. Ito, S. Kuwabata, H. Yoneyama, *Environ. Sci. Technol.*, **1996**, 30, 1275–1281.
- [12] M. Toyoda, Y. Nanbu, T. Kito, M. Hiranob, M. Inagaki, *Desalination*, **2003**, 159, 273–282.
- [13] A. Bhattacharyya, S. Kawi, M. B. Ray, *Catal. Today*, **2004**, 98, 431–439.
- [14] M. Mahalakshmi, S. Vishnu Priya, B. Arabindoo, M. Palanichamy, V. Murugesan, *J. Hazard. Mater.*, **2009**, 161, 336–343.
- [15] A. C. Pierre, G. M. Pajonk, *Chem. Rev.*, **2002**, 102, 4243–4266.
- [16] H. L. Wang, W. Z. Liang, W. F. Jiang, *Mater. Chem. Phys.*, **2011**, 130, 1372–1379.
- [17] S. Sankararaman, K. B. Yoon, T. Yabe, J. K. Kochi, *J. Am. Chem. Soc.*, **1991**, 113, 1419–1421.
- [18] A. N. Ökte, Ö. Yılmaz, *Appl. Catal. B*, **2008**, 85, 92–102.
- [19] T. Horiuchi, L. Y. Chen, T. Osaki, T. Sugiyama, K. Suzuki, T. Mori, *Catal. Lett.*, **1999**, 58, 89–92.
- [20] P. B. Sarawade, J. K. Kim, H. K. Kim, H. T. Kim, *Appl. Surf. Sci.*, **2007**, 254, 574–579.
- [21] H. Tamon, T. Sone, M. Okazaki, *J. Colloid Interf. Sci.*, **1997**, 188, 162–167.
- [22] R. S. Iyer, J. A. Scott, *Resour. Conserv. Recycl.*, **2001**, 31, 217–228.
- [23] Y. F. Jia, B. Xiao, K. M. Thomas, *Langmuir*, **2002**, 18, 470–478.
- [24] H. L. Wang, S. Q. Liu, X. Y. Zhang, *J. Hazard. Mater.*, **2009**, 169, 448–453.
- [25] H. J. Jeon, S. C. Yi, S. G. Oh, *Biomaterials*, **2003**, 24, 4921–4928.
- [26] M. Łączka, K. Cholewa-Kowalska, M. Kogut, *J. Non-Cryst. Solids*, **2001**, 287, 10–14.
- [27] A. Mills, R. H. Davies, D. Worsley, *Chem. Soc. Rev.*, **1993**, 22, 417–425.
- [28] M. Nikazar, K. Gholivand, K. Mahanpoor, *Desalination*, **2008**, 219, 293–300.
- [29] C. Anderson, A. J. Bard, *J. Phys. Chem. B*, **1997**, 101, 2611–2616.

Page numbers refer to the contents in the print version, which include both the English version and extended Chinese abstract of the paper. The online version only has the English version. The pages with the extended Chinese abstract are only available in the print version.